Response of Tropical Terrestrial Gross Primary Production to the Super El Niño Event in 2015

Jiawen Zhu[1,2], Minghua Zhang[1,2], Yao Zhang[3], Xiaodong Zeng[1,4], and Xiangming Xiao[5]

Correspondence to: J. Zhu, zhujw@mail.iap.ac.cn

Abstract

The gross primary production (GPP) in tropical terrestrial ecosystems plays a critical role in the global carbon cycle and climate change. The strong 2015–2016 El Niño event offers a unique opportunity to investigate how GPP in the tropical terrestrial ecosystems responds to climatic forcing. This study uses two GPP products and concurrent climate data to investigate the GPP anomalies and their underlying causes. We find that both GPP products show an enhanced GPP in 2015 for the tropical terrestrial ecosystem as a whole relative to the multiyear mean of 2001–2015, and this enhancement is the net result of GPP increase in tropical forests and decrease in nonforests. We show that the increased GPP in tropical forests during the El Nino event is consistent with increased photosynthesis active radiation as a result of a reduction in clouds, while the decreased GPP in nonforests is consistent with increased water stress as a result of a reduction of precipitation and an increase of temperature. These results reveal the strong coupling of ecosystem and climate that is different in forest and nonforest ecosystems and provide a test case for carbon cycle parameterization and carbon-climate feedback simulation in models.

1 Introduction

Tropical terrestrial ecosystems play a significant role in the global carbon cycle and climate change. The gross primary production (GPP) of these systems accounts for about 60% of the global land GPP (Beer et al., 2010), which contributes to a large fraction of fixation of atmospheric carbon dioxide (CO_2). How GPP of the tropical terrestrial ecosystem responds to climate change is a subject of intense research because the magnitude of carbon-climate feedback can strongly affect future climate change.

During the last several decades, tropical terrestrial ecosystems have shown evidential changes in response to rising atmospheric CO_2 and climate change (Baker et al., 2004; Lewis et al., 2009; Pan et al., 2011). Studies based on inventory plots reported an increase in old-growth forests carbon storage over Amazonia and Africa during recent decades (Baker et al., 2004; Lewis et al., 2009; Pan et al., 2011), which acts to slow down the increasing atmospheric CO_2 concentration and associated climate warming. Model simulations also showed net tropical land uptake for four different future emission scenarios (Sitch et al., 2008). Many processes on ecosystem response to climate change, however, remain poorly understood because of the short duration of available observational data and highly uncertain

models (Huntingford et al., 2013; Restrepo-Coupe et al., 2013; Smith et al., 2016).

Several studies used the observed seasonality and interannual variability in the land carbon cycle of tropical terrestrial ecosystems to understand the underlying mechanism of ecosystem response to climate change. Wang et al. (2013) analyzed the relationships between global average atmospheric CO_2 and annual mean temperature and precipitation over the tropics. They reported the stronger and more persistent control of temperature than precipitation on the tropical land carbon cycle. Fang et al. (2017) examined the response of tropical land carbon fluxes to El Niño-Southern Oscillation and concluded temperature being the key factor following El Niño years but precipitation being the dominant driver post La Niña years. Several studies showed that the increased solar radiation results in higher greenness and stronger photosynthetic activity of central Amazon forests during dry months than during wet months (Guan et al., 2015; Hilker et al., 2014; Huete et al., 2006; Saleska et al., 2016). Others showed that water supply is the key factor that controls the photosynthetic activity of forests along southern Amazonia and adjacent savannah (Guan et al., 2015; Hilker et al., 2014; Restrepo-Coupe et al., 2013). According to the estimation of Zhao and Running (2010), large tropical vegetated land areas had decreased net primary production from 2000 to 2009 because of drought. Seddon et al. (2016) assessed the sensitivity of terrestrial ecosystems to climate variability and found that there are significant heterogeneities in the responses of tropical terrestrial ecosystems to variability in air temperature, water availability, and solar radiation. These studies all point to the strong response of tropical terrestrial ecosystems to climate variability but also suggest that this response could be different with respect to different aspects of climate change and ecosystem traits.

The super 2015–2016 El Niño provides natural experiments to investigate the response of tropical terrestrial photosynthesis metabolism to climate variability (Liu et al., 2017). The 2015–2016 was the strongest El Niño event on record, with longer time and farther west than the 1997–1998 El Niño (Huang et al., 2016). Its influences on terrestrial carbon cycle are largely different from those of the 1997–1998 El Niño (Wang et al., 2018). Recently published studies have reported a “green-up” of Amazon forests in response to the 2015–2016 El Niño event through using a variety of data sets, including the enhanced vegetation index (EVI), leaf area index (LAI), and the fraction of absorbed photosynthesis active radiation (fPAR; Li et al., 2018; Yang et al., 2018). Meanwhile, paradoxically, they also showed reduced photosynthesis of Amazon forests during the 2015–2016 El Niño from the analysis of solar-induced chlorophyll fluorescence (SIF) from the Global Ozone Monitoring Experiment-2.

The objective of this study is to investigate the response of the tropical terrestrial ecosystem to the 2015–2016 El Niño event and its underlying causes by using recently available GPP products. We show how GPP in the

tropical terrestrial system as a whole responds and how forest and nonforest ecosystems respond differently to the El Nino event. We also analyze the associated dominant drivers and processes.

2 Data Sets and Methods

2.1 Climate Data Sets

We used surface temperature, precipitation, potential evapotranspiration (PET), and photosynthesis active radiation (PAR) as our climate data. Monthly surface temperature and precipitation are from the Climatic Research Unit-National Centers for Environmental Prediction (CRU-NCEP), downloaded from input data of the Community Earth System Model in National Center for Atmospheric Research (https://svn-ccsm-inputdata.cgd.ucar.edu/trunk/inputdata). The data set spans from 1901 to 2016 and is at 0.5° horizontal resolution. The data set has been used in several previous studies to investigate the responses of the tropical ecosystems carbon cycle to El Niño-Southern Oscillation (Fang et al., 2017; Piao et al., 2014; Wang et al., 2013, 2014). The PET was obtained from CRU TS v4.01 (http://doi.org/10/gcmcz3; Harris & Jones, 2017). This PET also covers the period from 1901 to 2016, with 0.5° horizontal resolution.

We obtained PAR in synoptic top of atmosphere and surface fluxes and clouds (SYN) Edition 4 from the National Aeronautics and Space Administration (NASA) Langley Research Center, Cloud and Earth's Radiant Energy System (https://ceres.larc.nasa.gov; Wielicki et al., 1996). This data set is at 1° spatial resolution and monthly temporal resolution from March 2000 to the present. The total PAR was calculated as the sum of surface direct and diffusive PAR in the all-sky conditions (Li et al., 2018; Yang et al., 2018).

The cloud fraction was downloaded from the NASA Earth Observation (https://neo.sci.gsfc.nasa.gov). This data set is from the Moderate Resolution Imaging Spectroradiometer (MODIS) cloud product collected from the Terra platform (MOD06; Platnick et al., 2015). This data set is at 0.5° spatial resolution and monthly temporal resolution from February 2000 to present.

2.2 Gross Primary Production

We used two independent GPP products in this study. The first is the MODIS GPP product (MOD17A2H.006; Running et al., 2015; hereafter GPP_{MOD17}), downloaded from NASA's Land Processes Distributed Active Archive Center (https://lpdaac.usgs.gov) located at the United States Geological Survey Earth Resources Observation and Science Center. The GPP_{MOD17} estimates GPP values based on light use efficiency theory and is widely used (Running et al., 2004). The GPP_{MOD17} is at 0.5-km spatial and 8-day temporal resolution from February 2000 to present and was interpolated into 0.5° spatial resolution and aggregated to monthly average in this study.

The second is a GPP product (hereafter GPP_{VPM}) estimated by the vegetation photosynthesis model (VPM) with an improved light use efficiency theory (Zhang et al., 2016, 2017). The GPP_{VPM} shows satisfactory performance when compared to site-level validations across large different biome types (Xiao et al., 2005). The GPP_{VPM} provides multiple spatial and temporal resolutions over the globe spanning from 2000 to 2016. In this study, we employed monthly GPP_{VPM} at 0.5° horizontal resolution.

There are inherent uncertainties for both GPP_{MOD17} and GPP_{VPM} (Running & Zhao, 2015; Zhang et al., 2017). First, both GPP_{MOD17} and GPP_{VPM} are dependent on MODIS land cover type. A misclassification of land cover type can occur in areas with complex vegetation at 0.5-km scale. Second, uncertainties are introduced by the assumption that biome-specific physiological parameters remain constant with space or time for GPP_{MOD17} and the treatment of C3/C4 plants for GPP_{VPM}. Third, GPP_{MOD17} is dependent on LAI and fPAR, and GPP_{VPM} is dependent on EVI. All the three variables may be contaminated by clouds and aerosols. Fourth, climate data sets used to drive GPP_{MOD17} and GPP_{VPM} contain uncertainties because of sparse weather stations and small-scale convection processes.

In addition to the two GPP products, we also downloaded the shorter record of another GPP product from NASA's National Snow and Ice Date Center (https://nsidc.org). This GPP product is estimated by using a satellite data-based terrestrial carbon flux model informed by Soil Moisture Active Passive (SMAP) L-band microwave observations, land cover and vegetation inputs from MODIS, Visible Infrared Imaging Radiometer Suite, and the Goddard Earth Observing System Model, Version 5, land model assimilation system (Kimball et al., 2017). This is a daily GPP product (hereafter GPP_{SMAP}), which covers the period from 31 March 2015 to present at a spatial resolution 9 km by 9 km.

2.3 Enhanced Vegetation Index

To investigate if the GPP response is based on vegetation response, we downloaded and analyzed the EVI data set from MODIS (MOD13C2.006; Didan, 2015; hereafter EVI_{MOD13}). The EVI_{MOD13} has improved its sensitivity in regions with high biomass. The EVI_{MOD13} is at 0.05° spatial and monthly temporal resolution from February 2000 to present and was interpolated into 0.5° spatial resolution in this study.

2.4 Methods

We define tropical vegetated land in this study as areas between latitudes 30°N and 30°S where LAI in each month exceeds 0.01 based on land surface data from MODIS (Lawrence & Chase, 2007). We divide the vegetated area into two types, forests and nonforests, because of their significant different traits (Figure S1).

The 2015 anomalies of climate and GPP are calculated relative to the mean from 2001 to 2015. Since GPP_{MOD17} in December of 2015 is missed, its

anomalies are calculated based on the first 11 months. The interannual variation during 2001 to 2015 is used to obtain the standard deviation and to judge the statistical significance of the 2015 anomalies.

To evaluate the uncertainties of GPP_{MOD17} and GPP_{VPM}, we downloaded FLUX observations from FLUXNET2015 Data (http://fluxnet.fluxdata.org/). We chose sites GF-Guy (DOI: 10.18140/FLX/1440165) and ZA-Kru (DOI: 10.18140/FLX/1440188) because they are grouped as evergreen broadleaf forests and savannas, respectively, and they cover longer time than other tropical sites. More information about the two sites is summarized in Table S1. We chose values of GPP_{MOD17} and GPP_{VPM} in grids that are the nearest to the sites to compare with FLUX observations.

3 Results and Discussion

3.1 Climate Anomalies

In response to the super El Niño event in 2015, the tropical vegetated land experienced a severely warm and dry condition. The land-surface air temperature was 1.82 times the standard deviation (SD; 0.31°) higher than the 15-year mean of 2001–2015. Spatial patterns of surface air temperature anomalies in 2015 show warmer conditions in South America, West Africa, East Africa, South Africa, Southeast Asia, equatorial Asia, and western and eastern Australia (Figure 1a). Meanwhile, the tropical terrestrial annual mean precipitation in 2015 was 2.1 SD (101 mm/year) less than the 15-year mean precipitation. Regions with negative precipitation anomalies include large areas of South America, West Africa, South Africa, equatorial Asia, and Southeast Asia (Figure 1b).

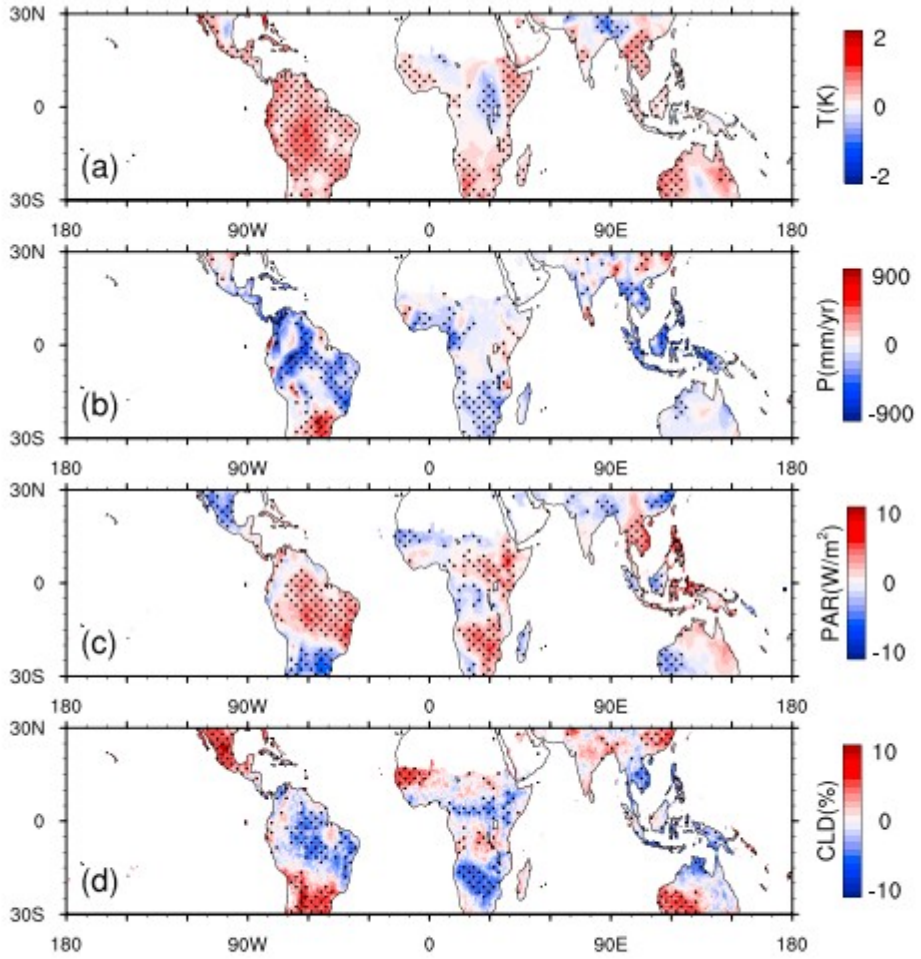

Figure 1. Spatial distributions of annual anomalies in (a) surface air temperature (K), (b) precipitation (P; mm/year), (c) photosynthesis active radiation (PAR; W/m^2), and (d) cloud fraction (CLD; %) of 2015 relative to the 15-year mean of 2001–2015. The stippled regions represent regions with anomalies larger than one interannual standard deviation.

Corresponding to the dry conditions, the tropical terrestrial annual PAR in 2015 increased by 1.3 SD (0.7 W/m^2) relative to the 15-year mean, with large contributions from regions including central and eastern South America, South Africa, East Africa, Southeast Asia, equatorial Asia, and northern and eastern Australia (Figure 1c). The increased PAR is consistent with the reduction of cloud cover over the tropical continents (Figure 1d), which is related to the reduction of precipitation in these regions. These climate anomalies are consistent with previous studies based on other climate data sets (Li et al., 2018; Liu et al., 2017; Yang et al., 2018), which together demonstrate the severely warm and dry conditions during 2015 over the tropics, as well as the increased PAR.

3.2 Response of GPP

Annual total GPP anomalies in 2015 relative to the 15-year averages are shown in Figure 2 for the tropical terrestrial ecosystem as a whole and for tropical America, Africa, and Asia. GPP_{MOD17} and GPP_{VPM} for the whole tropics

increased in 2015 by 0.10 SD (0.09 PgC/year) and 0.98 SD (1.00 PgC/year), respectively, relative to their 15-year averages. Tropical Asia contributes the largest to the positive 2015 GPP anomalies, with 0.79 PgC/year (1.53 SD) and 0.95 PgC/year (2.06 SD) in GPP_{MOD17} and GPP_{VPM}, respectively. This is followed by tropical America, with 0.17 PgC/year (0.37 SD) and 0.28 PgC/year (0.45 SD), respectively. In contrast, the 2015 GPP anomalies were negative for tropical Africa, with amplitudes of 0.88 PgC/year (2.71 SD) and 0.23 PgC/year (0.38 SD) in GPP_{MOD17} and GPP_{VPM}, respectively. In terms of percentages in different regions, the 2015 anomalies represent 5.0% and 3.5% of the total climatological GPP in tropical Asia in GPP_{MOD17} and GPP_{VPM}, respectively. The magnitudes of the percentages are the least in tropical America. The different percentage changes in different regions reflect the differences in the ecosystem traits and the magnitude of El Niño impact of climate.

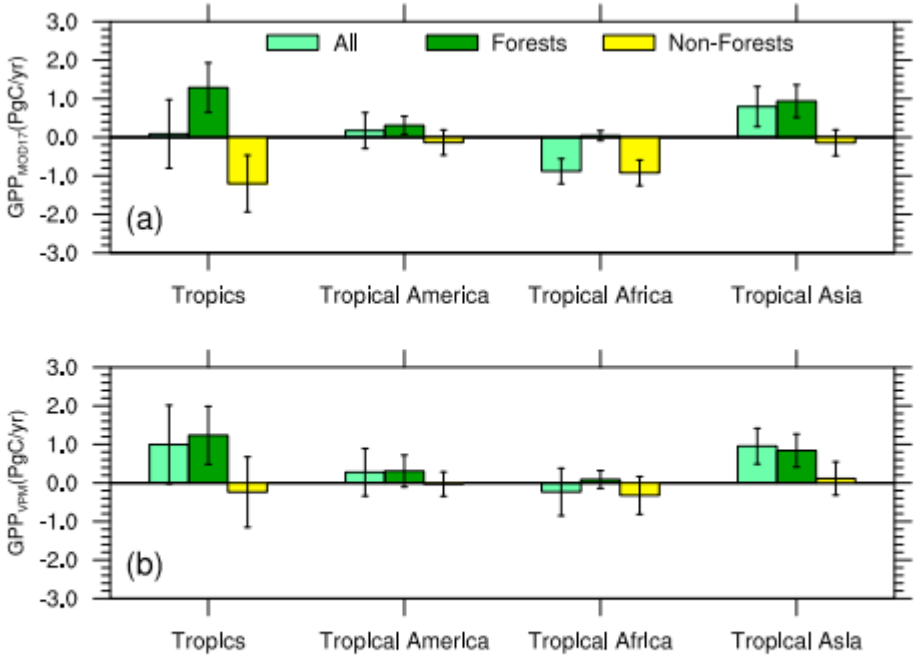

Figure 2. Total anomalies in (a) GPP_{MOD17} and (b) GPP_{VPM} (PgC/year) of 2015 relative to the 15-year mean of 2001–2015 for all grids (light green bars), forests-dominated (dark green bars) grids, and nonforests-dominated (yellow bars) grids over the whole tropics, tropical America, Africa, and Asia. The bars represent one standard deviation.

The two GPP products showed overall opposite response of tropical forest and nonforest GPP in 2015 relative to the 15-year mean (Figure **2**). GPP_{MOD17} and GPP_{VPM} for forests in the whole tropics increased in 2015 by 2.00 SD (1.29 PgC/year) and 1.64 SD (1.24 PgC/year), respectively, relative to their 15-year averages. Tropical Asia contributes the largest to the enhanced forest GPP in 2015, with 0.94 PgC/year (2.22 SD) and 0.84 PgC/year (1.96 SD) in GPP_{MOD17} and GPP_{VPM}, respectively. In contrast, GPP_{MOD17} and GPP_{VPM} for nonforests in the whole tropics decreased in 2015 by 1.64 SD (1.20 PgC/year) and 0.26 SD (0.24 PgC/year), respectively, relative to their 15-year averages. Tropical Africa contributes the largest to the decreased nonforest

GPP in 2015, with −0.92 PgC/year (−2.78 SD) and −0.32 PgC/year (−0.66 SD) in GPP_{MOD17} and GPP_{VPM}, respectively. These large differences between GPP_{MOD17} and GPP_{VPM} anomalies for nonforests in tropical Africa consequently result in large differences in GPP anomalies between the two products for the whole tropics (Figure **2**).

The spatial pattern of annual GPP anomalies in 2015 further shows that regions dominated by forests were generally characterized with enhanced GPP, including Amazon, central Africa, equatorial Asia, and Southeast Asia, while regions dominated by nonforests were generally with negative GPP anomalies, mainly over eastern South America, West Africa, South Africa, and northeastern Australia (Figure **3**). This feature is seen in both GPP products (Figures **3**a and **3**b). Since El Niño is generally associated with increased temperature, reduced precipitation, and increased PAR over the tropical continents as shown in Figure **1** regardless of the surface vegetation types, the GPP anomalies in Figures **2** and **3** strongly suggest that forests and nonforests have responded differently to the 2015 El Nino event.

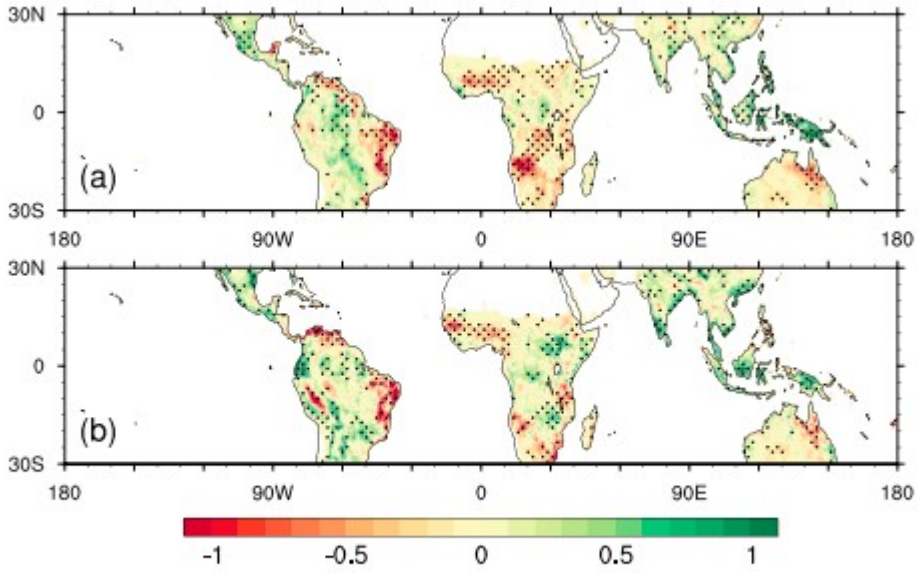

Figure 3. Spatial patterns of (a) GPP_{MOD17} and (b) GPP_{VPM} anomalies ($gC \cdot m^{-2} \cdot day^{-1}$) in 2015 relative to the 15-year mean of 2001–2015. The stippled regions represent regions with anomalies larger than one interannual standard deviation.

This difference can be more clearly seen by using the monthly anomalies of total GPP separately for forests and nonforests (Figure 4). In both products, forest GPP in 2015 is larger than climatology (Figures 4a and 4b), while nonforest GPP is smaller than climatology (Figures 4c and 4d) except for January in GPP_{VPM}. Positive and negative anomalies with magnitudes larger than the interannual SD are seen for forests and nonforests, especially in GPP_{MOD17}. The anomalies in GPP_{MOD17} are larger than those in GPP_{VPM}, and their seasonal variability is quite different for nonforests, which reflects the inherent uncertainties in the data products. Figure S2 shows that seasonal variability of the two GPP products for nonforests in tropical Africa is similar

with those shown in Figures 4c and 4d, which reflects more inherent uncertainties in the two products in tropical Africa as shown in Figure 2.

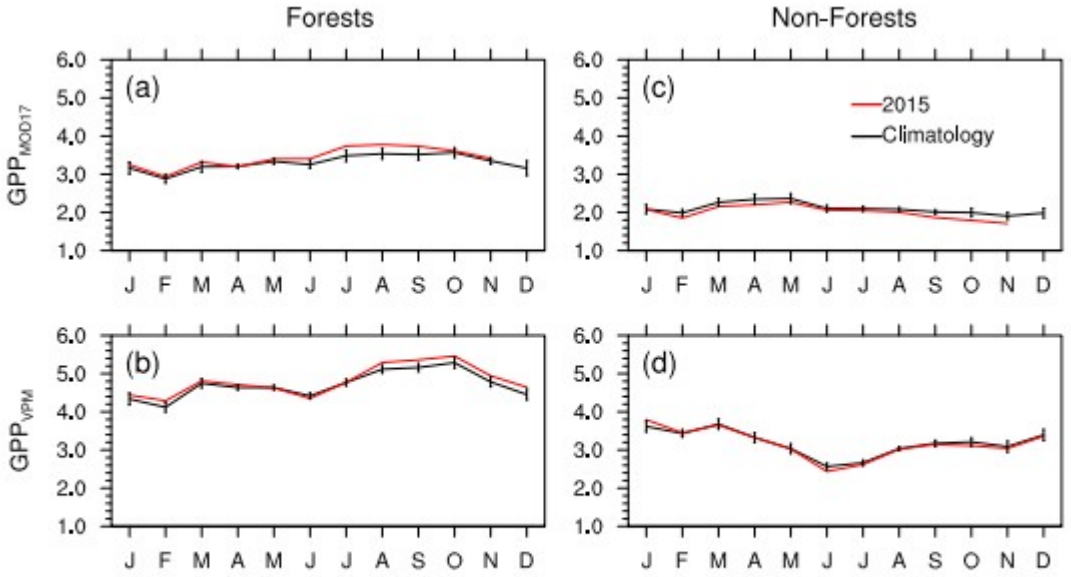

Figure 4. Seasonal variations in (a) GPP_{MOD17} (PgC/month) and (b) GPP_{VPM} (PgC/month) of 2015 (red lines) and the 15-year mean of 2001–2015 (black lines) in tropical forests-dominated regions. (c and d) Same as (a) and (b), respectively, but in tropical nonforests-dominated regions. The bars represent one standard deviation.

In addition to the two GPP products, we also examined the shorter record of GPP_{SMAP}, which has similar GPP anomalies in 2015 relative to the years 2016 and 2017 (Figure S3). EVI_{MOD13} shows positive EVI anomalies in 2015 in 12 months for tropical forests (Figure 5f) and negative EVI anomalies in 2015 in 4 months for tropical nonforested areas (Figure 5l), relative to the multiyear average of 2001–2015. This indicates that the above GPP anomalies for forests are mainly based on vegetation response and are more reliable than those for nonforested areas. The uncertainties will be discussed in section 3.4.

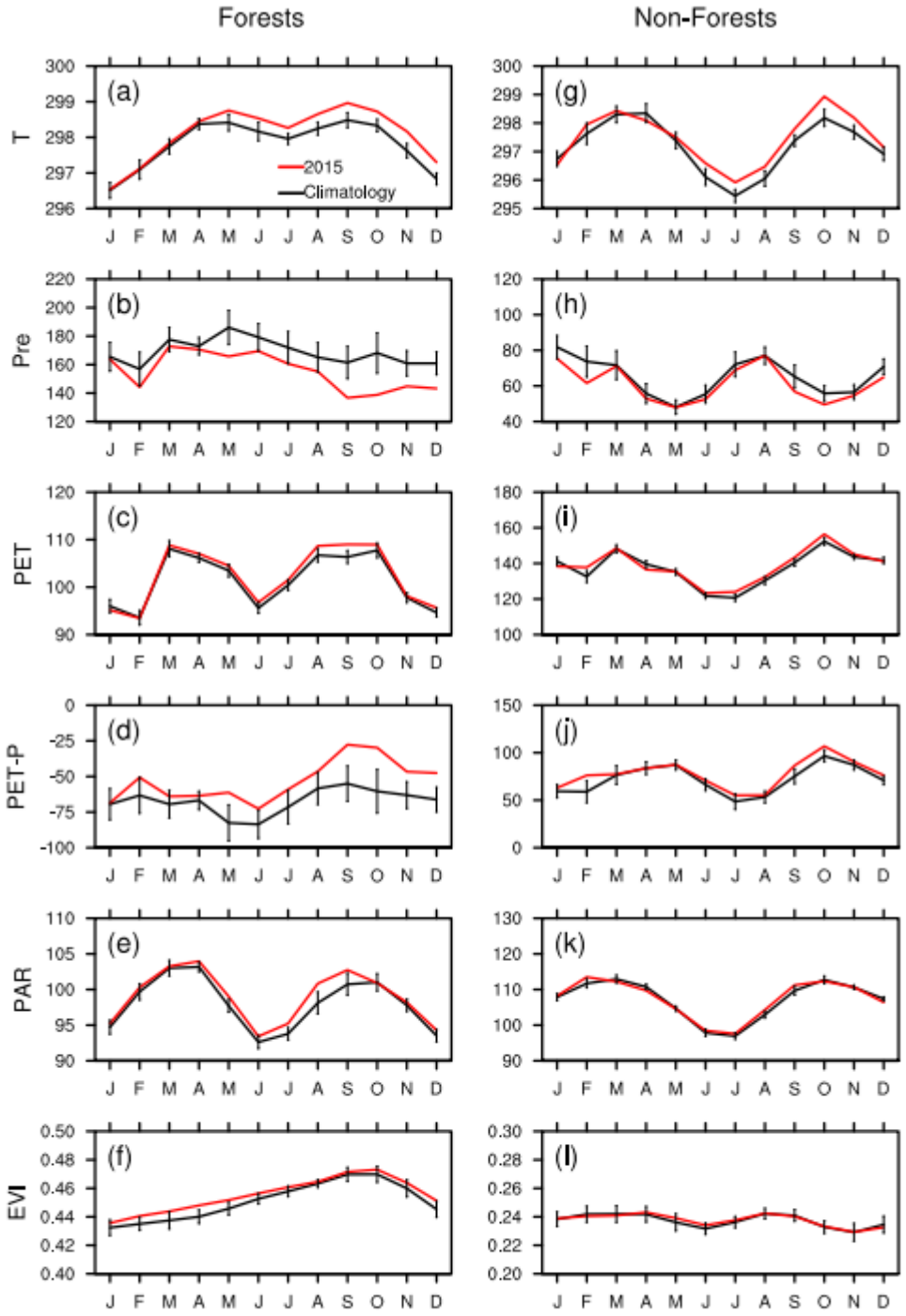

Figure 5. Seasonal variations in (a) surface temperature (K), (b) precipitation (Pre; mm/month), (c) potential evapotranspiration (PET; mm/month), (d) water stress (PET-P; mm/month), (e) photosynthesis active radiation (PAR; W m^{-2}); and (f) enhanced vegetation index (EVI) of 2015 (red lines) and the 15-year mean of 2001–2015 (black lines) in tropical forests-dominated regions. (g–l) Same as (a–f), respectively, but in tropical nonforests-dominated regions. The bars represent one standard deviation.

According to Le Quéré et al. (2018), the global land carbon sink decreased by 1.34 PgC in 2015, compared with the multiyear average of 2001–2015 (Figure S4). This means that ecosystem respiration may have also increased in the 2015 El Niño event and play an important role in annual net carbon

balance (Wang et al., 2018). Besides, Figure S4 also shows that in 2015 fossil fuel and industry emissions, land use emissions, and tropical fire carbon emissions increased by 1.23, 0.22, and 0.14 PgC, respectively, relative to the multiyear mean of 2001–2015 (Le Quéré et al., 2018). These sources together lead to an increase in the observed atmospheric CO_2 growth rate in 2015.

3.3 Coupling Between Climate and GPP Anomalies

We next show the corresponding climate variables separately for regions of forests and nonforests (Figure 5). These variables include surface temperature, precipitation, PET, and PAR. GPP is known to depend on PAR, precipitation and PET for water supply, and temperature. Large PAR favors great GPP due to photosynthesis, so does larger values of precipitation minus PET due to the great water supply. The temperature dependence of GPP is subtler because different vegetation types have a different optimal range of temperature for growth, but indirectly higher temperature leads to larger PET and larger water stress. Figure 5 shows that during the 2015 El Nino event, forests and nonforests both experienced warm anomalies in temperature, less than normal precipitation, larger PET, and larger PAR. The increased PAR should lead to more GPP, while the increased water stress as expressed by PET minus precipitation and increased temperature should lead to less GPP. These effects act to offset each other, and the dominant effect can be different in different ecosystems.

Over forests, the positive anomaly of GPP in 2015 suggests that the enhanced PAR played the dominant role in the ecosystem response. For forests in the three tropical continents, the monthly anomalies of GPP_{MOD17} in 2015 were significantly and positively correlated with the monthly PAR anomalies (Table S2). There are at least two reasons that can explain why the opposite effect of the water supply is relatively small. First, tropical forests have relatively high drought resistance because their deep roots can access seasonally redistributed subsurface water storage during the dry season (Giardina et al., 2018; Guan et al., 2015; Nepstad et al., 1994; Saleska et al., 2007). Second, as shown in Figure 5, even though precipitation is reduced (Figure 5b) and PET is increased (Figure 5c) in 2015, precipitation over tropical forests is still larger than PET (Figure 5d). Therefore, water stress for tropical forests was not very strong during the El Niño event.

Over nonforests, the negative anomaly of GPP in 2015 suggests that water stress and temperature played the dominant role in the ecosystem response. For nonforests in the four regions with largely decreased GPP (Figure S5), the monthly anomalies of GPP_{VPM} in 2015 were negatively correlated with the monthly anomalies in water stress and temperature (Table S2). The dominance of water stress over PAR for nonforest ecosystems is likely because the vegetation has shallower roots and are more sensitive to water stress, where PET is also larger than precipitation (Figure 5j).

3.4 Data Uncertainties and Perspective

A recent study, based on SIF from the Greenhouse gases Observing SATellite (GOSAT), reported a decreased tropical terrestrial GPP in 2015 relative to 2011 (Liu et al., 2017). Reduced Amazon forests photosynthesis has also been reported based on SIF data sets from Global Ozone Monitoring Experiment-2 during the 2015–2016 El Niño event (Li et al., 2018; Yang et al., 2018), although the decreased SIF signal may be caused by the artifacts of the data sets because of instruments degradation (Zhang et al., 2018a). These reports are contradictory to the results presented here.

To address the uncertainties of the two GPP products, we compare them with FLUXNET2015 data (GPP_{FLUX}) at sites GF-Guy (evergreen broadleaf forests) and ZA-Kru (savannas), which represent forests and nonforests, respectively. Figure 6 shows their seasonal variations.

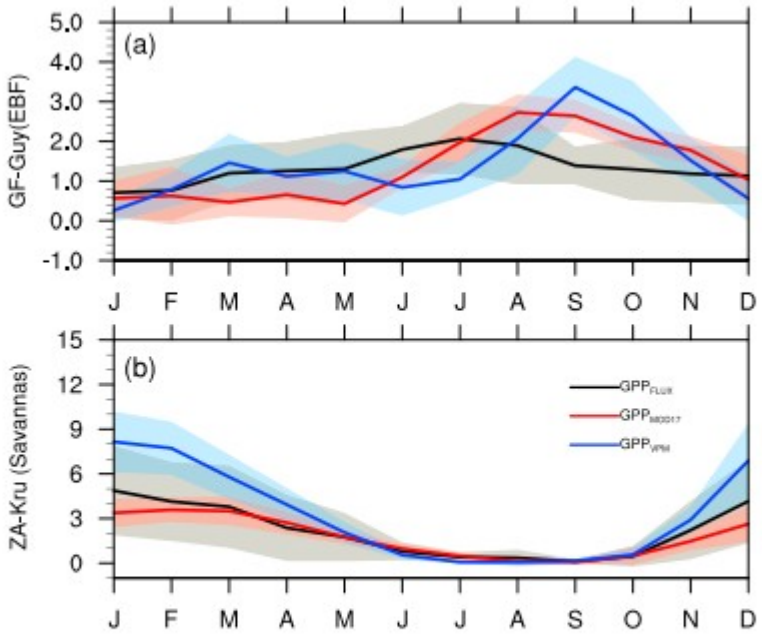

Figure 6. Seasonal variations of GPP_{FLUX} (black lines), GPP_{MOD17} (red lines), and GPP_{VPM} (blue lines) at sites (a) GF-Guy and (b) ZA-Kru. Values are deserved by calculating differences between the GPP of each month and the minimum GPP of corresponding 12 months at each year. Lines represent the multiyear mean of 2004–2014 for (a) and 2000–2009 for (b), and the shaded areas represent one standard deviation. All units are $gC \cdot m^{-2} \cdot day^{-1}$. GPP = gross primary production; EBF = evergreen broadleaf forests.

At site GF-Guy (Figure 6a), GPP_{FLUX} is the largest in July, while GPP_{MOD17} and GPP_{VPM} are the largest in August and September, respectively. Besides, the seasonal amplitudes of GPP_{MOD17} and GPP_{VPM} are larger than that of GPP_{FLUX}. These differences reflect uncertainties of the two GPP products in their sensitivity to climate variability for forests, and these uncertainties can result from many sources as shown in section 2. Generally, GPP_{FLUX} increases from January to July (Figure 6a), corresponding to an increase in solar radiation (Figure 7a), while GPP_{FLUX} decreases after July because of drought and high temperature. The lagged responses of the two GPP products indicate that

they may have a relatively high resistance to drought and high temperature for tropical forests. This characteristic results in uncertainties in amplitudes of the GPP anomalies for tropical forests shown above.

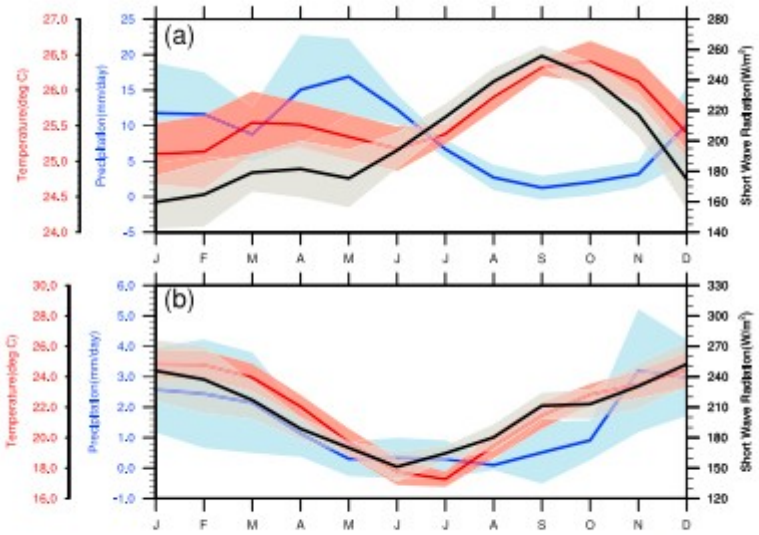

Figure 7. Seasonal variations of temperature (°C, red lines), precipitation (mm, blue lines), and shortwave radiation (W/m^2, black lines) at sites (a) GF-Guy and (b) ZA-Kru. Lines represent the multiyear mean of 2004–2014 for (a) and 2000–2009 for (b), and the shaded areas represent one standard deviation.

At site ZA-Kru, relative to GPP_{FLUX}, GPP_{MOD17} shows smaller seasonal amplitude, while GPP_{VPM} shows larger seasonal amplitude (Figure 6b). As above results show, with respect to other two tropical continents, tropical Africa also had the largest differences between GPP_{MOD17} and GPP_{VPM} for nonforests, including the amplitude (Figure 2) and seasonal variability (Figure S2). Figure S6 shows that C3/C4 plants grow over a large area of tropical Africa, and their photosynthetic processes are quite different. Therefore, the uncertainties of the two GPP products in the treatment of C3/C4 plants may result in uncertainties in the GPP anomalies for tropical nonforests shown above.

Despite these uncertainties, this work provides a valuable test case for understanding the response of tropical terrestrial ecosystems to climate variability. First, the results show strong coupling between tropical terrestrial ecosystems and climate that is largely different in tropical forest and nonforest ecosystems. Second, the inherent uncertainties in the two products reveal that more improvements are needed for the parameterization of land carbon cycle. The changes in the key driver of land carbon cycle in different seasons should be carefully considered. Third, more long-term simultaneous observations over the tropics are needed to provide more reliable information and to help us to understand the land carbon cycle for different ecosystems. Overall, our results point to the need to make more effort to investigate the coupling of tropical terrestrial ecosystems and climate, which is essential for accurately predicting the carbon-climate feedback under future climate change.

4 Summary

This study investigated the response of tropical terrestrial GPP to the warm and dry conditions in the super El Niño year 2015 and examined the associated dominant drivers and processes. Two independent GPP products, VPM and MODIS, both showed positive GPP anomalies over the tropics as a whole in 2015 relative to the 15-year mean from 2001 to 2015. We have also shown that GPP is enhanced over tropical forests but decreased in tropical nonforests in the 2015 El Niño event under the same climate anomalies of warmer temperature, less precipitation, larger PET, and larger PAR. We argued that the enhancement of GPP over forests is an indication of the dominant role of increased PAR in the 2015 El Niño event, while reduced GPP over nonforests is an indication of the dominant impact of high temperature and water stress as a result of reduced precipitation and increased PET. The difference in the response of GPP between forests and nonforests can be explained by the different water storage and stress of the two types of ecosystems.

The differences between tropical forests and nonforests reveal the complicity of climate-carbon relationship and indicate possible different risks that tropical vegetation may face climate change in different regions. Our results provide a case study to understand the underlying mechanisms about interactions between climate and tropical terrestrial ecosystems and to evaluate GPP parameterization as well as carbon-climate feedback in models.

Acknowledgments

This study is supported by grant 2016YFB02008 of the National Major Research High-Performance Computing Program of China, grant 41705070 of the National Natural Science Foundation of China and by the U.S. Department of Energy's Earth System Modeling (CMDV) program. We thank the National Center for Atmospheric Research for providing CRU-NCEP surface temperature and precipitation (https://svn-ccsm-inputdata.cgd.ucar.edu/trunk/inputdata); Harris, I. C., and Jones, P. D., for providing CRU TS v4.01 potential evapotranspiration (http://doi.org/10/gcmcz3); NASA's Cloud and Earth's Radiant Energy System for providing photosynthesis active radiation (https://ceres.larc.nasa.gov); NASA Earth Observation for providing monthly cloud product (https://neo.sci.gsfc.nasa.gov); NASA's Land Processes Distributed Active Archive Center for providing MODIS GPP (https://lpdaac.usgs.gov) and EVI; Prof. Xiangming Xiao and Dr. Yao Zhang for providing VPM GPP (https://figshare.com/collections/A_global_moderate_resolution_dataset_of_gross_primary_production_of_vegetation_for_2000-2016/3789814/1); NASA's National Snow and Ice Date Center for providing SMAP GPP (https://nsidc.org); and FLUXNET2015 data set (http://fluxnet.fluxdata.org/). We also appreciate the anonymous reviewers for their comments that significantly improve the quality of the paper.

References

Baker, T. R., Phillips, O. L., Malhi, Y., Almeida, S., Arroyo, L., Di Fiore, A., et al. (2004). Increasing biomass in Amazonian forest plots. *Philosophical Transactions of the Royal Society of London. Series B, Biological Sciences*, 359(1443), 353– 365. https://doi.org/10.1098/rstb.2003.1422

Beer, C., Reichstein, M., Tomelleri, E., Ciais, P., Jung, M., Carvalhais, N., Rodenbeck, C., Arain, M. A., Baldocchi, D., Bonan, G. B., Bondeau, A., Cescatti, A., Lasslop, G., Lindroth, A., Lomas, M., Luyssaert, S., Margolis, H., Oleson, K. W., Roupsard, O., Veenendaal, E., Viovy, N., Williams, C., Woodward, F. I., & Papale, D. (2010). Terrestrial gross carbon dioxide uptake: Global distribution and covariation with climate. *Science*, 329(5993), 834–838. https://doi.org/10.1126/science.1184984

Didan, K. (2015). MOD13C2 MODIS/Terra vegetation indices monthly L3 global 0.05Deg CMG V006 [data set]. NASA EOSDIS LP DAAC. https://doi.org/10.5067/MODIS/MOD13C2.006

Fang, Y. Y., Michalak, A. M., Schwalm, C. R., Huntzinger, D. N., Berry, J. A., Ciais, P., et al. (2017). Global land carbon sink response to temperature and precipitation varies with ENSO phase. *Environmental Research Letters*, 12(6), 10. https://doi.org/10.1088/1748-9326/aa6e8e

Giardina, F., Konings, A. G., Kennedy, D., Alemohammad, S. H., Oliveira, R. S., Uriarte, M., & Gentine, P. (2018). Tall Amazonian forests are less sensitive to precipitation variability. *Nature Geoscience*, 11(6), 405– 409. https://doi.org/10.1038/s41561-018-0133-5

Guan, K. Y., Pan, M., Li, H. B., Wolf, A., Wu, J., Medvigy, D., et al. (2015). Photosynthetic seasonality of global tropical forests constrained by hydroclimate. *Nature Geoscience*, 8(4), 284– 289. https://doi.org/10.1038/ngeo2382

Harris, I.C., & Jones, P.D. (2017). CRU TS4.01: Climatic Research Unit (CRU) Time-Series (TS) version 4.01 of high-resolution gridded data of month-by-month variation in climate (Jan. 1901- Dec. 2016). Centre for Environmental Data Analysis, 04 December 2017. https://doi.org/10.5285/58a8802721c94c66ae45c3baa4d814d0

Hilker, T., Lyapustin, A. I., Tucker, C. J., Hall, F. G., Myneni, R. B., Wang, Y. J., et al. (2014). Vegetation dynamics and rainfall sensitivity of the Amazon. *Proceedings of the National Academy of Sciences of the United States of America*, 111(45), 16,041– 16,046. https://doi.org/10.1073/pnas.1404870111

Huang, B. Y., L'heureux, M., Hu, Z. Z., & Zhang, H. M. (2016). Ranking the strongest ENSO events while incorporating SST uncertainty. *Geophysical Research Letters*, 43, 9165– 9172. https://doi.org/10.1002/2016GL070888

Huete, A. R., Didan, K., Shimabukuro, Y. E., Ratana, P., Saleska, S. R., Hutyra, L. R., Yang, W., Nemani, R. R., & Myneni, R. (2006). Amazon rainforests

green-up with sunlight in dry season. *Geophysical Research Letters*, 33, L06405. https://doi.org/10.1029/2005GL025583

Huntingford, C., Zelazowski, P., Galbraith, D., Mercado, L. M., Sitch, S., Fisher, R., Lomas, M., Walker, A. P., Jones, C. D., Booth, B. B. B., Malhi, Y., Hemming, D., Kay, G., Good, P., Lewis, S. L., Phillips, O. L., Atkin, O. K., Lloyd, J., Gloor, E., Zaragoza-Castells, J., Meir, P., Betts, R., Harris, P. P., Nobre, C., Marengo, J., & Cox, P. M. (2013). Simulated resilience of tropical rainforests to CO_2-induced climate change. *Nature Geoscience*, 6(4), 268– 273. https://doi.org/10.1038/ngeo1741

Kimball, J. S., Jones, L. A., Glassy J., & Reichle R. (2017). SMAP L4 global daily 9 km carbon net ecosystem exchange, Version 3. [Indicate subset used]. Boulder, Colorado USA. NASA National Snow and Ice Data Center Distributed Active Archive Center. https://doi.org/10.5067/O4HAQJEWWUU8

Lawrence, P. J., & Chase, T. N. (2007). Representing a new MODIS consistent land surface in the Community Land Model (CLM 3.0). *Journal of Geophysical Research*, 112, G01023. https://doi.org/10.1029/2006JG000168

Le Quéré, C., Andrew, R. M., Friedlingstein, P., Sitch, S., Pongratz, J., Manning, A. C., et al. (2018). Global carbon budget 2017. *Earth System Science Data*, 10(1), 405– 448. https://doi.org/10.5194/essd-10-405-2018

Lewis, S. L., Lopez-Gonzalez, G., Sonke, B., Affum-Baffoe, K., Baker, T. R., Ojo, L. O., et al. (2009). Increasing carbon storage in intact African tropical forests. *Nature*, 457(7232), 1003– 1006. https://doi.org/10.1038/nature07771

Li, X., Xiao, J. F., & He, B. B. (2018). Higher absorbed solar radiation partly offset the negative effects of water stress on the photosynthesis of Amazon forests during the 2015 drought. *Environmental Research Letters*, 13(4), 044005.

Liu, J., Bowman, K. W., Schimel, D. S., Parazoo, N. C., Jiang, Z., Lee, M., Bloom, A. A., Wunch, D., Frankenberg, C., Sun, Y., O'Dell, C. W., Gurney, K. R., Menemenlis, D., Gierach, M., Crisp, D., & Eldering, A. (2017). Contrasting carbon cycle responses of the tropical continents to the 2015–2016 El Niño. *Science*, 358(6360), eaam5690. https://doi.org/10.1126/science.aam5690

Nepstad, D. C., Decarvalho, C. R., Davidson, E. A., Jipp, P. H., Lefebvre, P. A., Negreiros, G. H., et al. (1994). The role of deep roots in the hydrological and carbon cycles of amazonian forests and pastures. *Nature*, 372(6507), 666– 669. https://doi.org/10.1038/372666a0

Pan, Y. D., Birdsey, R. A., Fang, J. Y., Houghton, R., Kauppi, P. E., Kurz, W. A., et al. (2011). A large and persistent carbon sink in the world's forests. *Science*, 333(6045), 988– 993. https://doi.org/10.1126/science.1201609

Piao, S., Nan, H., Huntingford, C., Ciais, P., Friedlingstein, P., Sitch, S., et al. (2014). Evidence for a weakening relationship between interannual

temperature variability and northern vegetation activity. *Nature Communications*, 5(5018). https://doi.org/10.1038/ncomms6018

Platnick, S., Ackerman, S. A., King, M. D., Meyer, K., Menzel, W. P., Holz R. E., et al. (2015). MODIS atmosphere L2 cloud product (06_L2), NASA MODIS Adaptive Processing System, Goddard Space Flight Center dx. https://doi.org/10.5067/MODIS/MOD06_L2.006

Restrepo-Coupe, N., Da Rocha, H. R., Hutyra, L. R., Da Araujo, A. C., Borma, L. S., Christoffersen, B., et al. (2013). What drives the seasonality of photosynthesis across the Amazon basin? A cross-site analysis of eddy flux tower measurements from the Brasil flux network. *Agricultural and Forest Meteorology*, 182, 128– 144. https://doi.org/10.1016/j.agrformet.2013.04.031

Running, S. W., Mu, Q., & Zhao, M. S. (2015). MOD17A2H MODIS/Terra gross primary productivity 8-day L4 global 500m SIN grid V006 [Data set]. NASA EOSDIS Land Processes DAAC. https://doi.org/10.5067/MODIS/MOD17A2H.006

Running, S. W., Nemani, R. R., Heinsch, F. A., Zhao, M. S., Reeves, M., & Hashimoto, H. (2004). A continuous satellite-derived measure of global terrestrial primary production. *Bioscience*, 54(6), 547– 560. https://doi.org/10.1641/0006-3568(2004)054[0547:ACSMOG]2.0.CO;2

Running, S. W., & Zhao, M. S. (2015). User's Guide: Daily GPP and annual NPP (MOD17A2/A3) products NASA Earth Observing System MODIS Land Algorithm.

Saleska, S. R., Didan, K., Huete, A. R., & Da Rocha, H. R. (2007). Amazon forests green-up during 2005 drought. *Science*, 318(5850), 612– 612. https://doi.org/10.1126/science.1146663

Saleska, S. R., Wu, J., Guan, K. Y., Araujo, A. C., Huete, A., Nobre, A. D., & Restrepo-Coupe, N. (2016). Dry-season greening of Amazon forests. *Nature*, 531(7594), E4– E5. https://doi.org/10.1038/nature16457

Seddon, A. W. R., Macias-Fauria, M., Long, P. R., Benz, D., & Willis, K. J. (2016). Sensitivity of global terrestrial ecosystems to climate variability. *Nature*, 531(7593), 229– 232. https://doi.org/10.1038/nature16986

Sitch, S., Huntingford, C., Gedney, N., Levy, P. E., Lomas, M., Piao, S. L., et al. (2008). Evaluation of the terrestrial carbon cycle, future plant geography and climate-carbon cycle feedbacks using five Dynamic Global Vegetation Models (DGVMs). *Global Change Biology*, 14(9), 2015– 2039. https://doi.org/10.1111/j.1365-2486.2008.01626.x

Smith, W. K., Reed, S. C., Cleveland, C. C., Ballantyne, A. P., Anderegg, W. R. L., Wieder, W. R., et al. (2016). Large divergence of satellite and Earth system model estimates of global terrestrial CO_2 fertilization. *Nature Climate Change*, 6(3), 306– 310. https://doi.org/10.1038/nclimate2879

Wang, J., Zeng, N., Wang, M., Jiang, F., Wang, H., & Jiang, Z. (2018). Contrasting terrestrial carbon cycle responses to the 1997/98 and 2015/16 extreme El Niño events. *Earth System Dynamics*, 9(1), 1– 14. https://doi.org/10.5194/esd-9-1-2018

Wang, W. L., Ciais, P., Nemani, R. R., Canadell, J. G., Piao, S. L., Sitch, S., et al. (2013). Variations in atmospheric CO_2 growth rates coupled with tropical temperature. *Proceedings of the National Academy of Sciences of the United States of America*, 110(32), 13,061– 13,066. https://doi.org/10.1073/pnas.1219683110

Wang, X. H., Piao, S. L., Ciais, P., Friedlingstein, P., Myneni, R. B., Cox, P., et al. (2014). A two-fold increase of carbon cycle sensitivity to tropical temperature variations. *Nature*, 506(7487), 212– 215. https://doi.org/10.1038/nature12915

Wielicki, B. A., Barkstrom, B. R., Harrison, E. F., Lee, R. B., Smith, G. L., & Cooper, J. E. (1996). Clouds and the Earth's Radiant Energy System (CERES): An Earth observing system experiment. *Bulletin of the American Meteorological Society*, 77(5), 853– 868. https://doi.org/10.1175/1520-0477(1996)077<0853:CATERE>2.0.CO;2

Xiao, X. M., Zhang, Q. Y., Saleska, S., Hutyra, L., De Camargo, P., Wofsy, S., et al. (2005). Satellite-based modeling of gross primary production in a seasonally moist tropical evergreen forest. *Remote Sensing of Environment*, 94(1), 105– 122. https://doi.org/10.1016/j.rse.2004.08.015

Yang, J., Tian, H. Q., Pan, S. F., Chen, G. S., Zhang, B. W., & Dangal, S. (2018). Amazon drought and forest response: Largely reduced forest photosynthesis but slightly increased canopy greenness during the extreme drought of 2015/2016. *Global Change Biology*, 24(5), 1919– 1934. https://doi.org/10.1111/gcb.14056

Zhang, Y., Joiner, J., Gentine, P., & Zhou, S. (2018a). Reduced solar-induced chlorophyll fluorescence from GOME-2 during Amazon drought caused by dataset artifacts. *Global Change Biology*, 24(6), 2229– 2230. https://doi.org/10.1111/gcb.14134

Zhang, Y., Xiao, X. M., Jin, C., Dong, J. W., Zhou, S., Wagle, P., et al. (2016). Consistency between Sun-induced chlorophyll fluorescence and gross primary production of vegetation in North America. *Remote Sensing of Environment*, 183, 154– 169. https://doi.org/10.1016/j.rse.2016.05.015

Zhang, Y., Xiao, X. M., Wu, X. C., Zhou, S., Zhang, G. L., Qin, Y. W., & Dong, J. W. (2017). Data Descriptor: A global moderate resolution dataset of gross primary production of vegetation for 2000–2016. *Scientific Data*, 4(13). https://doi.org/10.1038/sdata.2017.165

Zhao, M. S., & Running, S. W. (2010). Drought-induced reduction in global terrestrial net primary production from 2000 through 2009. *Science*, 329(5994), 940– 943. https://doi.org/10.1126/science.1192666